

Supplementary Information for

Steering of guided light with dielectric nanoantennas

Ivan Sinev,^{1,*} Filipp Komissarenko,¹ Ivan Iorsh,¹ Dmitry
Permyakov,¹ Anton Samusev,¹ and Andrey Bogdanov¹

¹*Department of Physics and Engineering,
ITMO University St. Petersburg, Russia*

I. SCATTERING OF LIGHT FROM A SINGLE SILICON NANOSPHERE

Here, we present the compact version of the routine for analytical calculation of the silicon nanosphere polarizability and SPP directivity patterns. For a more detailed sequence, refer to *e.g.* Supplementary Materials for [1].

First, the full magnetic and electric dipole polarizabilities of a spherical silicon nanoparticle on top of gold are calculated using Green's function approach following the routine presented in detail in [2]. This method allows to straightforwardly calculate the Cartesian components of dipole moments induced in the nanosphere by an arbitrary polarized incident field with account for the substrate effects. Spectral dependences of gold and silicon dielectric permittivities that we use in the calculation are taken from [3] and [4], respectively.

After the calculation of the magnetic dipole \mathbf{m} and electric dipole \mathbf{p} induced in the nanosphere by the incident field, we proceed to obtain the directivity patterns of SPP induced on a gold substrate by such dipole source. The magnetic field induced by \mathbf{m} and \mathbf{p} can be represented through the dyadic Green's function:

$$\mathbf{H}(\mathbf{r}) = k_0^2 G_H(\mathbf{r})\mathbf{m} + ik_0 \nabla \times G_E(\mathbf{r})\mathbf{p}. \quad (1)$$

The explicit form of Green's function in this equation is calculated as a linear superposition of the incident and reflected plane waves and reads

$$G_H(\rho, \phi_0, 0) = G_H^{reg} + \frac{i}{8\pi^2} \iint k dk d\phi \frac{r_p(k)}{k_z} \begin{pmatrix} \sin^2 \phi & -\cos \phi \sin \phi & 0 \\ -\cos \phi \sin \phi & \cos^2 \phi & 0 \\ 0 & 0 & 0 \end{pmatrix} e^{ik\rho \cos(\phi-\phi_0) + ik_z h}, \quad (2)$$

$$\begin{aligned} \nabla \times G_E(r, \phi_0, 0) &= \nabla G_E^{reg} - \\ &- \frac{1}{8\pi^2} \iint k dk d\phi \frac{r_p(k)}{k_z} \begin{pmatrix} \sin 2\phi k_z/2 & \sin^2 \phi k_z & k \sin \phi \\ -\cos^2 \phi k_z & -\sin 2\phi k_z/2 & -k \cos \phi \\ 0 & 0 & 0 \end{pmatrix} e^{ik\rho \cos(\phi-\phi_0) + ik_z h}, \end{aligned} \quad (3)$$

where $k_z = \sqrt{k_0^2 - k^2}$, and $r_p(k) = (k_z - k_{zm}/\varepsilon_m)/(k_z + k_{zm}/\varepsilon_m)$ is the magnetic field reflection coefficient for the TM-polarized plane wave with $k_{zm} = \sqrt{\varepsilon_m k_0^2 - k^2}$, where ε_m is

the metal dielectric permittivity, and h is the sphere radius. Here, we have separated the Green's function into the regular and singular part. The regular part of the Green's function contains the incident field and the contribution from the TE-polarized reflected field. The regular part does not contribute to the SPP field, which originates from the pole of the reflection coefficient $r_p(k)$. The regular part is thus omitted in the following considerations.

The equation can be simplified considerably by using the Jacobi-Anger expansion of the form $\int_0^{2\pi} \cos n\phi e^{ix \cos \phi} = 2\pi(i)^n J_n(x)$, (here, $J_n(x)$ is the Bessel function of the first kind) and asymptotic relations for the resulting expressions.

After some algebra (please refer to Supplementary Materials of [1] for intermediate derivations), we arrive at the following equation for the induced magnetic field components (in the following, φ denotes the azimuthal angle, *i.e.* the direction of SPP excitation):

$$H_x \sim -(m_x k_0 + p_y k_z) \sin^2 \varphi + (m_y k_0 - k_z p_x) \sin \varphi \cos \varphi - k_{SPP} p_z \sin \varphi, \quad (4)$$

$$H_y \sim -(m_y k_0 - p_x k_z) \cos^2 \varphi + (k_z p_y + m_x k_0) \sin \varphi \cos \varphi + k_{SPP} p_z \cos \varphi, \quad (5)$$

$$H_\varphi = -H_x \sin \varphi + H_y \cos \varphi \sim (m_x k_0 + k_z p_y) \sin \varphi + (k_z p_x - m_y k_0) \cos \varphi + k_{SPP} p_z \quad (6)$$

The SPP field intensity is proportional to $|H_\varphi|^2$, which gives us the final equation calculation of the SPP directivity patterns (equation 1 in the main text), $\kappa = -i\sqrt{1/(\varepsilon_m + 1)}$, $\tilde{k}_{SPP} = \sqrt{\varepsilon_m/(\varepsilon_m + 1)}$:

$$I_{SPP}(\varphi) \sim \left| (m_x + i\kappa p_y) \sin \varphi + (m_y - i\kappa p_x) \cos \varphi - \tilde{k}_{SPP} p_z \right|^2, \quad (7)$$

Since the conditions for interference between electric and magnetic dipole moments are crucial for SPP beam steering effect discussed in the main text, we provide separate illustration of forward-to-backward switching conditions with the change of the wavelength of p-polarized excitation wave. Spectral dependence of the induced dipole moments and associated directivity spectra, calculated using the described approach, are shown in Fig. S1.

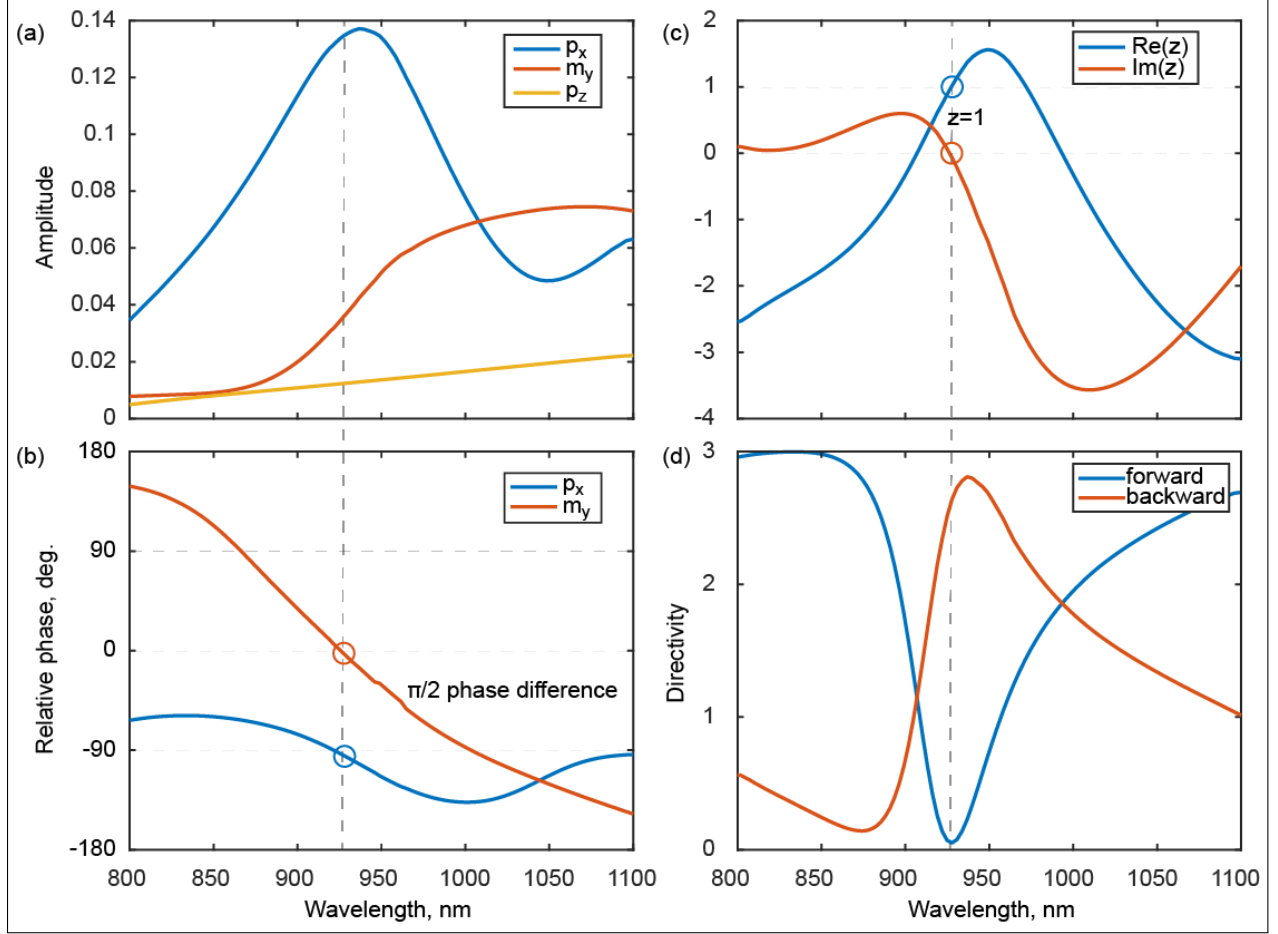


FIG. S1. (a) Spectral dependence of the amplitudes of the dipole moments induced in a 295 nm silicon nanosphere excited by a TM-polarized plane wave incident at 25 degrees. (b) Phase differences of the same dipole moments with respect to the slowly changing phase of p_z . (c) Spectral dependence of the real and imaginary part of the parameter $z = (m_y - ikp_x)/(\tilde{k}_{SPP}p_z)$ that characterizes the forward/backward switching condition for the excited SPP. (d) Spectral dependence of forward and backward directivity of the excited SPP. In all four panels, grey dashed line denotes the wavelength of total suppression of forward SPP scattering.

II. COMPARISON OF ANALYTICAL AND NUMERICAL CALCULATIONS OF SPP DIRECTIVITY

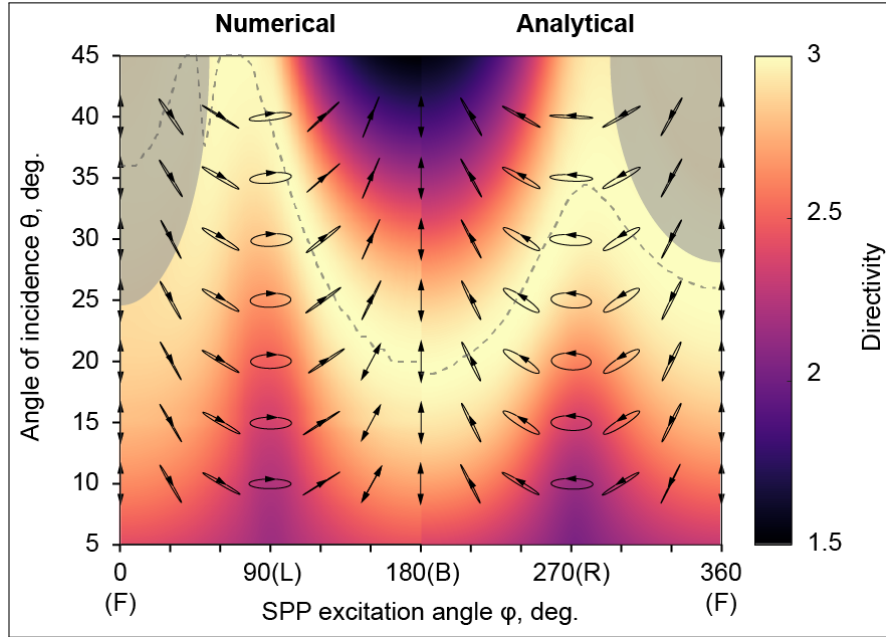


FIG. S2. Comparison of the maximum achievable SPP directivity from a 295 nm silicon nanosphere in numerical(left) and analytical (right) calculations. The directivity is encoded with false color. The overlay shows the polarization states of the incident light required to achieve the presented directivity values. Gray-shaded areas represent the geometries when maximum directivity is achieved at the boundary of the considered spectral range (1100 nm). Dashed lines track the condition of maximum directivity achieved for considered excitation parameters.

III. SPP FIELD DISTRIBUTION FOR LINEAR POLARIZATION

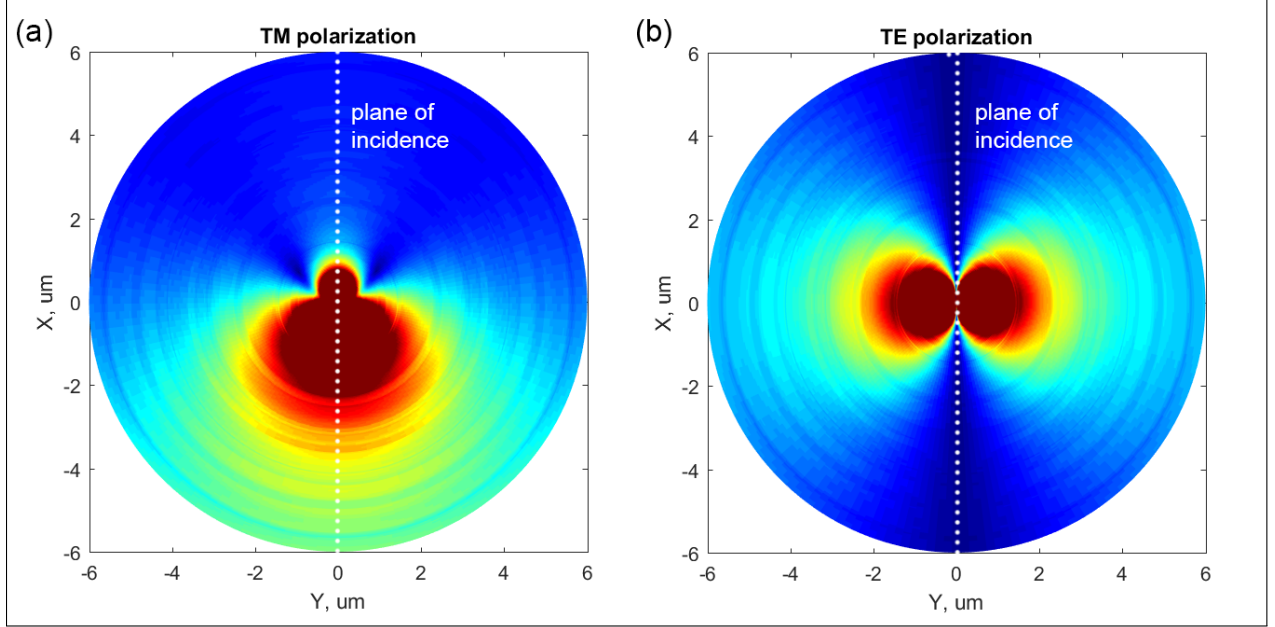


FIG. S3. SPP intensity profiles calculated for a 295 nm silicon nanosphere excited with linearly (a) TM- and (b) TE-polarized light. The wavelength of 940 nm is used as an example. Both intensity patterns are symmetric with respect to the plane of incidence (vertical axis).

IV. NUMERICAL SIMULATION OF THE SPP EXCITATION

For numerical simulation of SPP on Au air/interface excited by a Si sphere under oblique incident plane wave, we use COMSOL Multiphysics (2D axisymmetric domain, wave Optics module, frequency domain solver). The considered problem has a cylindrical symmetry, thus, the angular variable φ can be separated and both the incident and scattered field can be expanded into the following series:

$$\mathbf{E}_{\text{inc}}(\rho, \varphi, z) = \sum_{m=-\infty}^{\infty} \mathbf{E}_{\text{inc}}^m(\rho, z)e^{-im\varphi}. \quad (8)$$

Therefore, the problem can be reduced to 2D geometry that saves computing resources significantly and speeds up the calculations. We use the scattering formalism available in COMSOL, when the solution \mathbf{E}_{tot} is represented as a sum of the incident \mathbf{E}_{inc} and scattered

\mathbf{E}_{sc} fields:

$$\mathbf{E}_{\text{tot}} = \mathbf{E}_{\text{inc}} + \mathbf{E}_{\text{sc}}. \quad (9)$$

The problem under consideration is linear, thus, the scattered fields \mathbf{E}_{sc}^m for different azimuthal numbers m can be calculated independently and then summed. we limited ourselves to only azimuthal harmonics $m = -1, 0, 1$. Numerical analysis shows that higher azimuthal harmonics does not contribute much in the frequency range from 800 to 1100 nm.

We consider incident field of both TE (s) and TM (p) polarizations. The coordinate system and plane of incidence is shown in Fig. 3 (main text). The incident fields can be expanded in terms of the azimuthal harmonics as follows:

TM-polarization:

$$\mathbf{E}_{\text{inc}}^{\text{TM}} = \begin{pmatrix} E_{\rho}^{\text{TM}} \\ E_{\varphi}^{\text{TM}} \\ E_z^{\text{TM}} \end{pmatrix} e^{i\omega t + izk_0 \cos \theta - ixk_0 \sin \theta} = \begin{pmatrix} E_{\rho}^{\text{TM}} \\ E_{\varphi}^{\text{TM}} \\ E_z^{\text{TM}} \end{pmatrix} e^{i\omega t + izk_0 \cos \theta - ik_0 \rho \cos \varphi \sin \theta} \quad (10)$$

$$E_{\rho}^{\text{TM}} e^{-ik_0 \rho \cos \varphi \sin \theta} = E_0^{\text{TM}} \cos \theta \sum_{m=-\infty}^{+\infty} (-i)^{m+1} \frac{J_{m+1}(k_0 \rho \sin \theta) - J_{m-1}(k_0 \rho \sin \theta)}{2} e^{-im\varphi} \quad (11)$$

$$E_{\varphi}^{\text{TM}} e^{-ik_0 \rho \cos \varphi \sin \theta} = E_0^{\text{TM}} \cos \theta \sum_{m=-\infty}^{+\infty} (-i)^{m+2} \frac{J_{m+1}(k_0 \rho \sin \theta) + J_{m-1}(k_0 \rho \sin \theta)}{2} e^{-im\varphi} \quad (12)$$

$$E_z^{\text{TM}} e^{-ik_0 \rho \cos \varphi \sin \theta} = E_0^{\text{TM}} \sin \theta \sum_{m=-\infty}^{+\infty} (-i)^m J_m(k_0 \rho \sin \theta) e^{-im\varphi} \quad (13)$$

TE-polarization:

$$\mathbf{E}_{\text{inc}}^{\text{TE}} = \begin{pmatrix} E_{\rho}^{\text{TE}} \\ E_{\varphi}^{\text{TE}} \\ 0 \end{pmatrix} e^{i\omega t + izk_0 \cos \theta - ixk_0 \sin \theta} = \begin{pmatrix} E_{\rho}^{\text{TE}} \\ E_{\varphi}^{\text{TE}} \\ 0 \end{pmatrix} e^{i\omega t + izk_0 \cos \theta - ik_0 \rho \cos \varphi \sin \theta} \quad (14)$$

$$E_{\rho}^{\text{TE}} e^{-ik_0 \rho \cos \varphi \sin \theta} = -E_0^{\text{TE}} \sum_{m=-\infty}^{+\infty} (-i)^{m+2} \frac{J_{m+1}(k_0 \rho \sin \theta) + J_{m-1}(k_0 \rho \sin \theta)}{2} e^{-im\varphi} \quad (15)$$

$$E_{\varphi}^{\text{TE}} e^{-ik_0 \rho \cos \varphi \sin \theta} = E_0^{\text{TE}} \sum_{m=-\infty}^{+\infty} (-i)^{m+1} \frac{J_{m+1}(k_0 \rho \sin \theta) - J_{m-1}(k_0 \rho \sin \theta)}{2} e^{-im\varphi} \quad (16)$$

Here, θ is the angle of incidence, E_0^{TE} and E_0^{TM} are the amplitudes of the TE and TM-polarized incident waves. In the case of absence of nanoantenna, the total field consists of the incident, reflected and transmitted field, which can be found using Fresnel equations [5]. We use this total field as a background in the numerical model.

V. CALCULATION OF THE SPP EXCITATION EFFICIENCY

To estimate the SPP excitation efficiency during the steering, we calculated the cross section of scattering of the incident plane wave into SPP. The total power I of SPP far from the source ($|k_{\text{SPP}}\rho| \gg 1$) can be calculated straightforwardly by integration of the Poynting vector over the sidewall of an imagine cylinder concentric with the nanoantenna:

$$I \approx \frac{\pi |A^m|^2}{2\varepsilon_0\omega} \left[\frac{\text{Re}(k_{\text{SPP}}/\varepsilon_1)}{\text{Re}(\kappa_1)} + \frac{\text{Re}(k_{\text{SPP}}/\varepsilon_2)}{\text{Re}(\kappa_2)} \right] e^{2\text{Im}(k_{\text{SPP}})\rho}. \quad (17)$$

The indices 1 and 2 correspond to air (upper medium) and gold (lower medium). The coefficient A^m is the azimuthal component of the magnetic field of SPP (scattering amplitude) at the interface:

$$H_\varphi^m \approx A^m \frac{e^{-ik_\rho\rho}}{\sqrt{\rho}} e^{\mp\kappa_{1,2}z} e^{-im\varphi}$$

The exponential factor in (17) describes absorption of SPP in the metal. In order to find the total power of SPP via the scattering amplitude found numerically in COMSOL we need to compensate the exponential factor corresponding to absorption. The total excitation cross section of SPP can be obtained by division of the total power of SPP by the intensity of the incident field:

$$\sigma_{\text{SPP}} = I e^{-2\text{Im}(k_{\text{SPP}})\rho} / (|E_0|^2/2/Z_0).$$

Here E_0 is the amplitude of the incident electric field and Z_0 is the vacuum impedance.

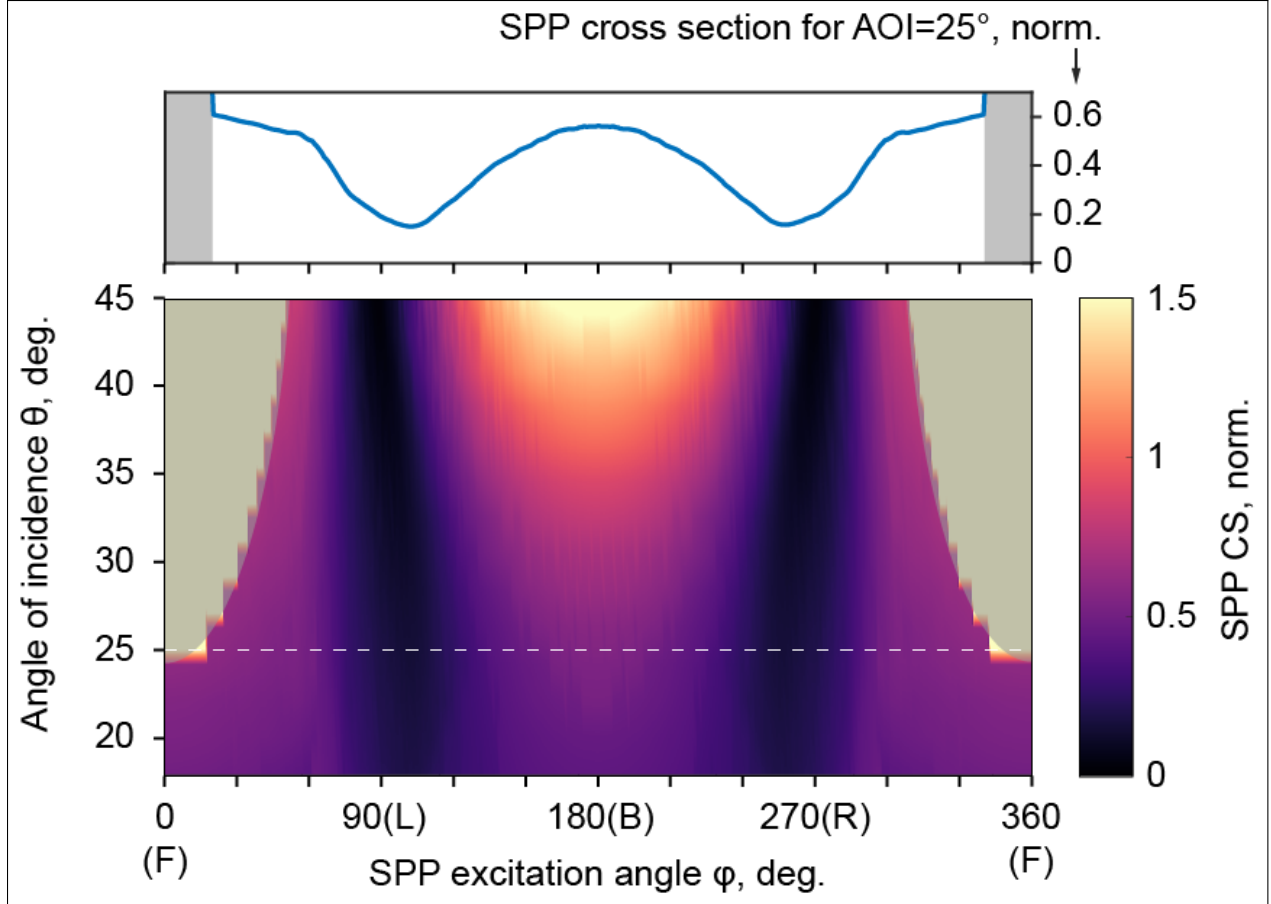


FIG. S4. Illustration of the efficiency of SPP excitation during the plasmonic beam steering. Top: SPP excitation cross section derived from the numerically calculated SPP fields from a 295 nm silicon nanoparticle on gold excited at the angle of incidence of 25 degrees. Bottom: cross section map for other angles of incidence. The excitation conditions (wavelength, polarization state) match those required to reach the maximum SPP directivity for each θ , φ (as illustrated in Fig. S2). The cross section values are normalized to the geometrical cross section of the nanoparticle ($\pi r^2 \approx 0.27 \mu m^2$). Shaded areas mark the conditions when the maximum directivity is achieved at the boundary of the considered spectral region (1100 nm). Dashed line denotes the section for $\theta=25$ shown in the top panel.

VI. VISUALIZATION OF SURFACE PLASMON POLARITON STEERING IN CALCULATION AND EXPERIMENT: DESCRIPTION OF SUPPLEMENT MOVIES S1-S3

Supplement Movie S1 illustrates the steering of SPP from a 295 nm silicon sphere on gold calculated with COMSOL Multiphysics for angle of incidence equal to 25 degrees. For each SPP direction, the excitation conditions (wavelength and polarization state) providing optimal directivity are shown in the top left quadrant. The SPP directivity patterns, field (H_φ) and SPP intensity profiles are shown in the other quadrants.

Supplement Movies S2 and S3 show the spectral evolution of experimentally measured directivity patterns of SPP from 295 nm silicon nanosphere for left and right circularly polarized excitation (angle of incidence is 25 degrees).

* i.sinev@metalab.ifmo.ru

- [1] Ivan S Sinev, Andrey A Bogdanov, Filipp E Komissarenko, Kristina S Frizyuk, Mihail I Petrov, Ivan S Mukhin, Sergey V Makarov, Anton K Samusev, Andrei V Lavrinenko, and Ivan V Iorsh, “Chirality driven by magnetic dipole response for demultiplexing of surface waves,” *Laser & Photonics Reviews* **11**, 1700168 (2017).
- [2] Andrey E. Miroshnichenko, Andrey B. Evlyukhin, Yuri S. Kivshar, and Boris N. Chichkov, “Substrate-induced resonant magnetoelectric effects for dielectric nanoparticles,” *ACS Photonics* **2**, 1423–1428 (2015).
- [3] P. B. Johnson and R. W. Christy, “Optical constants of the noble metals,” *Physical Review B* **6**, 4370–4379 (1972).
- [4] Martin A Green and Mark J Keevers, “Optical properties of intrinsic silicon at 300 k,” *Progress in Photovoltaics: Research and Applications* **3**, 189–192 (1995).
- [5] John David Jackson, *Classical electrodynamics* (AAPT, 1999).